Available online at www.sciencedirect.com
ScienceDirect
Nuclear Physics B Proceedings Supplement 00 (2014) 1–6
Nuclear Physics B Proceedings Supplement

Phase I Upgrade of the CMS Hadron Calorimeter

Seth I. Cooper on behalf of the CMS Collaboration

Abstract

In preparation for Run 2 (2015) and Run 3 of the LHC (2019), the CMS hadron calorimeter has begun a series of ambitious upgrades. These include new photodetectors in addition to improved front-end and back-end readout electronics. In the hadron forward calorimeter, the existing photomultiplier tubes are being replaced with thinner window, multi-anode readout models, while in the central region, the hybrid photodiodes will be replaced with silicon photomultipliers. The front-end electronics will include high precision timing readout, and the back-end electronics will handle the increased data bandwidth. The barrel and endcap longitudinal segmentation will also be increased. This report will describe the motivation for the upgrade, its major components, and its current status.

Keywords: CERN, LHC, CMS, calorimetry

1. Introduction

The Compact Muon Solenoid (CMS) experiment is one of four major detectors situated on the Large Hadron Collider (LHC) beamline, at the CERN lab, near Geneva, Switzerland [1]. During Run 1 of the LHC (through 2012), pp collisions occurred at a center of mass (CM) energy of up to 8 TeV with instantaneous luminosity of nearly 8×10^{33} cm^{-2} s^{-1} and up to 35 interactions per proton bunch crossing (pileup vertices). Proton bunches were spaced at 50 ns intervals. After Long Shutdown 1 (2013-2014), the LHC will begin to operate at 13 TeV CM energy with an instantaneous luminosity reaching as much as 2×10^{34} cm^{-2} s^{-1} and around 50 interactions per bunch crossing, with a bunch spacing of 25 ns. This Run 2 environment, especially with respect to the pileup, makes it a challenge to maintain good energy resolution in the calorimeters. In the case of the Hadron Calorimeter (HCAL), the Phase I upgrade should improve on the Run 1 performance, in addition to reducing anomalous signals observed in Run 1.

The HCAL is made up of four sections: Barrel (HB), Endcap (HE), Outer (HO), and Forward (HF). A diagram with the locations of the calorimeters in CMS is shown in Figure 1. The HB and HE are sampling calorimeters made of alternating layers of brass absorber and plastic scintillator [2]. The HO uses plastic scintillator and the CMS magnet material (e.g., iron return yoke) as the absorber [3]. In both cases, scintillation light is extracted with wavelength-shifting fibers, which illuminate individual pixels of a hybrid photodiodes (HPD). The HF is a Cherenkov calorimeter composed of steel absorber interspersed with longitudinally-running quartz core and acrylic clad fibers. The fibers are spaced at 5 mm, collecting the Cherenkov light produced by showers in the absorber [4]. The fibers in each η-ϕ tower are combined, with the light sent to a photomultiplier tube (PMT). All four HCAL components share similar front-end and back-end electronics. The analog HPD or PMT signal is integrated over 25 ns and digitized by the QIE8 chip in the front end [5]. The digitized signal values are continuously sent to the back-end electronics.

2. Upgrade Motivation and Overview

The HB, HE, HO, and HF each have their own motivations and timelines for upgrading. The main driver of the upgrade in the barrel, endcap, and outer calorimeters is the performance of the HPD. The HPD was chosen based on its high gain (greater than 2000) and magnetic

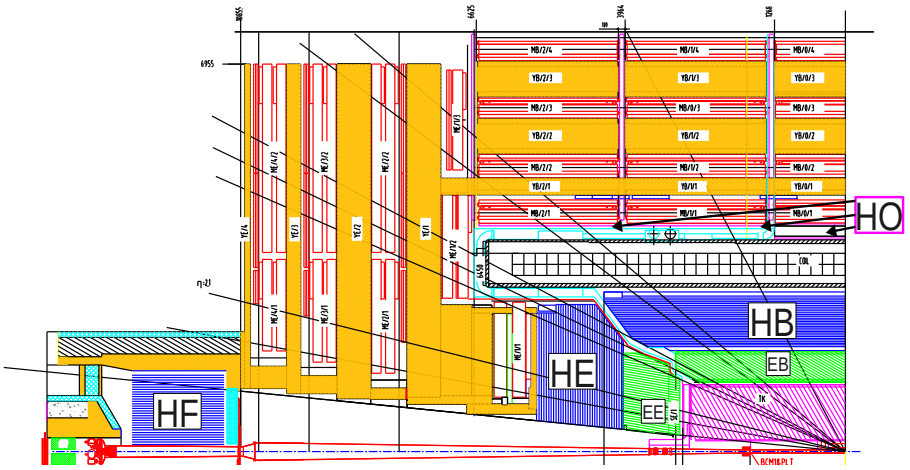

Figure 1: Locations of HCAL and electromagnetic (EB,EE) calorimeters in CMS in the r-z plane [6].

field tolerance. However, it requires a large electric field of 8 kV over a small gap of 3 mm. In Run 1, electrical discharges were observed, varying with the orientation and strength of the magnetic field with respect to the HPD. For HO, which experiences the fringe field, the effect was severe enough to warrant decreasing the high voltage by 1.5 kV in many channels. In addition to this effect, monitoring of the pixel response with an LED system showed divergence from unity as time passed. The complete gain variation mechanism is not understood, and the rate of variation has not slowed. For these reasons, the HPDs will be replaced with silicon photomultipliers (SiPMs). For HO, this is already occurring during LS1, the first long shutdown of the LHC, in 2013 and 2014.

In the HF, early operation in 2010 indicated the presence of anomalous signals due to hits on the PMT windows from muons or particle showers. The hits mimic very high energy deposits, which can be flagged topologically in the low-pileup environment of Run 1. With increasing luminosity, however, this becomes increasingly difficult, and another method of rejection is needed. These signals have the property of arriving early with respect to Cherenkov light from the fibers, so a timing-based rejection can be used. In Run 1, the phase of the HF readout was adjusted such that these early hits occurred in an empty bunch crossing immediately prior to that containing the collision. In Run 2, every bunch crossing will contain a collision, so that this method will no longer be possible. A multi-pronged upgrade approach is employed to keep these anomalous signals under control. The PMTs will be replaced, and new front-end electronics will be installed which will include precise timing measurements. Most of the components in this new front-end will be shared with those used in HB and HE to read out the SiPMs.

Finally, for HB, HE, and HF, new back-end electronics will be deployed, based on the MicroTCA standard [7]. The new back-ends will handle the resulting increased data volume (from, e.g., the front-end timing measurement) in addition to easing long-term maintenance.

3. HCAL Barrel and Endcap

As noted above, the major component of the HCAL barrel and endcap upgrade is the replacement of HPDs with SiPMs. The SiPM is an array of Geiger-mode operated avalanche photodiodes, divided into pixels of micron size. It operates with a low bias voltage of under 100 V, but has a high gain, on the order of 10^4. The devices are typically a few square millimeters in area, with tens of thousands of effective pixels. They exhibit a recovery time of less than 10 ns, ensuring that shifts in response from pileup events will be minimal.

The radiation tolerance of the SiPMs for both neutrons and ionizing particles was studied in detail at the IRRAD facility at CERN. The expected dose is 14 Gray ionizing radiation, and $7{\times}10^{11}$ cm^{-2} in 1 MeV neutrons, calculated using the CMS Dose-Fluence Calculator [8]. The requirements, including safety margins, are set at 100 Gray ionizing dose and $2{\times}10^{12}$ cm^{-2} neutrons. Neutron damage increases the SiPM leakage current by way of bulk damage. The leakage current, being primarily caused by pixel discharges, is coupled to the SiPM gain. Too much leakage current will initiate a

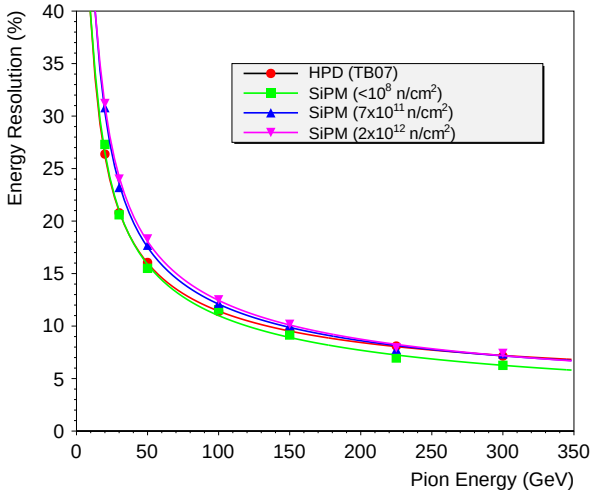

[htb]

Figure 2: Energy resolution as a function of pion energy for neutron-irradiated SiPMs (from simulations) compared to HPDs (from test beam data). A 1 mm^2 device is shown [6].

positive feedback loop of increased heating leading to higher leakage current, resulting in instability. An upper limit of 200 μA is set on the leakage current to preempt this issue. Figure 2 shows the SiPM response to radiation, and therefore leakage current, based on simulations. Test beam measurements of HPD response are also shown. Here, pions are used which deposit a negligible amount of energy in the CMS electromagnetic calorimeter, which sits in front of the HCAL. The SiPM can be seen to perform nearly as well as the HPD at high dose; the resolution degradation is very small compared with the overall energy resolution.

The higher signal-to-noise performance of the SiPM with respect to the HPD enables an increase in the longitudinal readout segmentation from 1 or 2 (at high eta) in the barrel to 3 and 2-3 (at high eta) in the endcap to 4 or 5. Recent developments in reconstructing hadronic showers using particle flow techniques can take advantage of these increases in segmentation. Finer segmentation will also allow for improved recalibration as radiation damage occurs at high pseudorapidity during Run 2, as channels at different depths can be read out and recalibrated separately. Figure 3 shows the increased depth segmentation division with scintillator layer.

4. HCAL Forward

Similarly to the barrel and endcap upgrade SiPM upgrade, the HF will also undergo a replacement of its photodetectors, in this case an upgrade to new photomultiplier tubes. These tubes have two main properties that will help mitigate the anomalous signals seen in Run 1: thinner optical windows and multi-anode output. The thinner windows were motivated by the fact that the signal produced in the PMT from a window hit is proportional to the path length through the window. Tests of the new PMTs at the CERN H2 testbeam, where particles were fired directly at the PMT, indicated that the reduction in window thickness reduced the anomalous signals by a factor of four.

The multi-anode readout will provide the ability to identify an anomalous signal and remove its energy in a particular readout channel, recovering the channel's normal response. This is due to the fact that light produced by the calorimeter (e.g., from a particle shower) will illuminate all photocathodes identically (within Poisson statistics) and produce signals in all anodes whereas a PMT hit will produce a signal in one anode only. Figure 4 shows an example algorithm developed on this principle using 2-anode readout, which can tag these PMT hits with around 90% efficiency and near-zero mis-tagging rate.

Finally, the upgraded front-end electronics (see below) will enable the readout of the additional anode channels in addition to providing a timing measurement with a built-in time to digital converter (TDC). The TDC will identify the signal arrival times with subnanosecond resolution, giving an additional method of identifying the ~5 ns early-arriving anomalous signals.

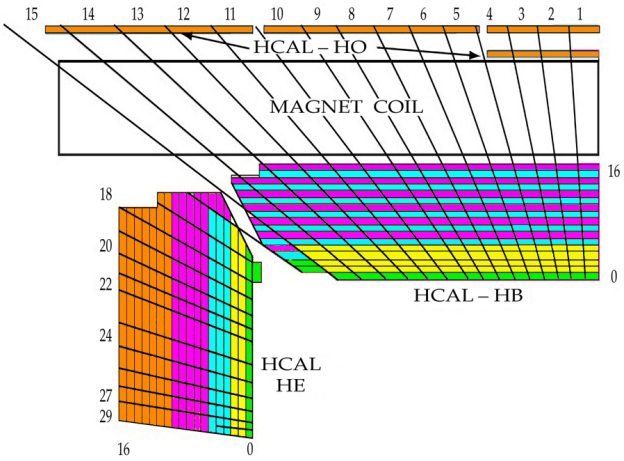

Figure 3: Possible depth segmentation in HB and HE using SiPMs [6].

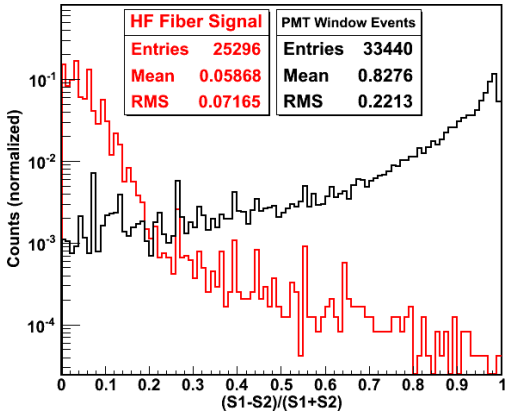

Figure 4: Identification variable for anomalous signals using two anode readout. S1 and S2 represent the signals in the two readout channels, with S1 > S2. Data collected from CERN H2 test beam. Black distribution is from particle hits on the PMT, while the red curve is from electron showers [6].

5. Front-End Electronics

As stated above, new front-end electronics will be deployed in Phase I (through Long Shutdown 2 in 2018) to support the increase in readout channels and to provide precision timing measurements. The new front-end is shared among HB, HE, and HF, and carries with it improved redundancy in the control system. A diagram of the front-end and back-end electronics is shown in Figure 5. A key component of the front-end is the charge integrator and encoder (QIE) ASIC. It integrates the charge in each 25 ns interval and digitizes it, with the data at each interval transmitted continuously to the back-end electronics. This strategy has been advantageous in Run 1, as any needed data processing modifications can be made in the back-end. A new QIE, version 10, is being developed for use in the upgraded front-ends. It has a large dynamic range, with a 3 fC least significant (LSB) bit up to 330 pC, which corresponds to 1.1 TeV in an HB/HE channel, or 33,000 SiPM photoelectrons. The LSB is larger than the SiPM RMS noise (2 fC) and allows good determination of the single photoelectron (10 fC) and MIP signals (~50 fC). The mantissa used is 6 bits, which is enough to keep the quantization error at the 3% level or below, smaller than the calorimeter resolution (see Figure 6).

Another main part of the front end is the clock and control ASIC used for alignment of the QIE data and clock transmission. In the upgraded front end, this and other ASICs will be replaced by commercial field-programmable gate arrays (FPGA). A flash-based FPGA will be used, rather than the more common static RAM based chips, due to better radiation hardness. In addition, the flash-based FPGAs have lower

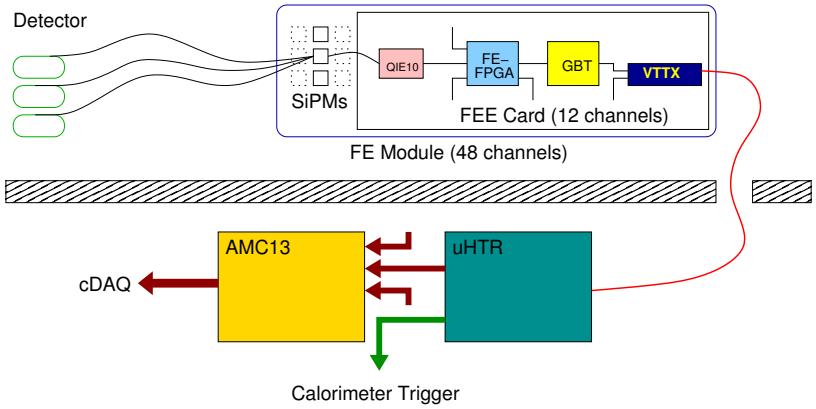

Figure 5: Flow of the data in HB/HE, from the SiPM through the QIE, data alignment in the FPGA, transmission to the back-end, and the AMC13 link to CMS central data acquisition [6].

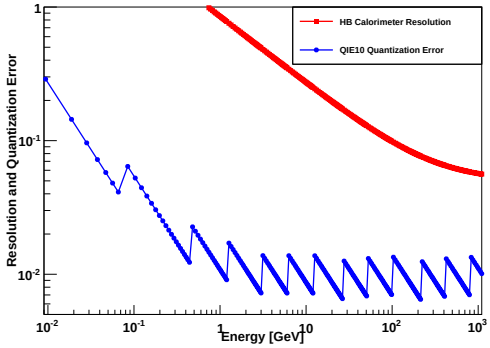

Figure 6: QIE10 quantization error (blue) compared with HCAL resolution. It can be seen that the quantization error is substantially smaller than the resolution over the entire energy range [6].

power consumption, are reprogrammable, and retain their data when switched off. Their radiation hardness has been extensively studied and is determined to be robust against various known negative effects and to the total ionizing dose expected.

Finally, a new clock and control system, dubbed the ngCCM, or next-generation clock and control module, will be deployed which will configure the other elements of the front end, deliver the clock, and provide signals such as a reset or for calibration use. The ngCCM is centered on a flash-based FPGA, and will also increase the robustness of this system over that used for Run 1. During Run 1 operation, the failure of a CCM would have resulted in a serious loss of readout channels, as there is no redundancy. To address this issue, in the ngCCM design an extra control path exists between each pair of ngCCMs. In the event of a failure of the main optical link between an ngCCM and the counting room, or of various ngCCM components, this alternate path can be used to recover control.

6. Back-End Electronics

The HCAL back-end electronics are responsible for receiving the continuous readout of front-end data, calculating and transmitting trigger information, storing and sending the front-end and trigger data on receipt of a Level-1 Accept from the CMS global trigger, operating in local data acquisition and triggering mode, and handling fast clock and control signals. The upgraded back-ends will be based on commercial FPGAs and the MicroTCA (μTCA) standard [7]. The main component of the HCAL back-end is the μHTR. In addition, a μTCA crate will contain an Advanced Mezzanine Card 13 (AMC13) which provides the link to the CMS central data acquisition (DAQ) system, including event building. The μHTR contains two Xilinx FPGAs, the front FPGA, which takes as input front-end data via parallel optical receivers, and the back FPGA, which transmits data to the central DAQ. The front FPGA performs the synchronization and pipelining of the data, in addi-

tion to calculating and transmitting the trigger information, while the back FPGA is responsible for buffering and applying zero suppression. The upgraded electronics will be able to provide significant improvements in the trigger, including increased granularity, and feature bits, e.g., based on TDC information. The μHTR-based back-end will be able to read out the upgraded and the existing front-end modules, and was tested with the existing front-ends during p-Pb collisions in 2013.

7. Schedule

The installation of the upgrade electronics will proceed in stages, to avoid deploying new front-ends and back-ends at the same time, thereby minimizing disruptions. In general, the back-end upgrades will be installed and commissioned before the new front-ends. During LS1, the HF PMT replacement will be completed and will be ready for multi-anode readout (available with the new front-ends). The HF μTCA back-ends will also be installed and commissioned in time for operations in 2015. This will allow the installation of the new HF front-end electronics during the year-end technical stop from late 2015 to early 2016.

For HB and HE, the upgraded back-ends will also be installed in 2014, with commissioning throughout 2015 and 2016 using split signals from the existing front-ends. The VME and μHTR backends will operate in parallel for a time until the existing calorimeter trigger is completely replaced with its planned upgraded version [9], at which point the VME electronics can be decommissioned. The complete HB and HE front-end replacement is scheduled for Long Shutdown 2 in 2018. Unlike HF, the HB and HE front-ends are only accessible when CMS is open, which typically does not occur during a year-end technical stop, due to the amount of work involved.

8. Conclusion

The HCAL Phase I upgrade was motivated by early observations of the HCAL performance, in addition to anticipating the needs for the harsh radiation, luminosity, and pileup environments expected in LHC Run 2. To improve upon the excellent HCAL performance in Run 1 requires a comprehensive upgrade plan involving all parts of the calorimeter. All photodetectors will be replaced, which will increase the reliability and decrease the rate of anomalous signals. The new front-end electronics will have better radiation tolerance, higher redundancy, and include new features such as signal timing information. They will also allow an increase in the depth segmentation in the barrel and endcap, and enable better background suppression in the forward calorimeter. The new back-ends will handle the increased data-volume, in addition to moving to the more modern components, simplifying long-term maintenance.

The HF PMT and back-end upgrade will be completed by the end of 2014, and the HB and HE back-end deployment will be in progress. The system will thus be ready for the installation and commissioning of the new front-ends, starting with HF at the end of 2015. With all the components in place, the upgraded HCAL will meet its goal of providing even better jet and missing energy measurements in spite of the more challenging Run 2 conditions.

References

[1] S. Chatrchyan, et al., The CMS experiment at the CERN LHC, JINST 3 (2008) S08004. doi:10.1088/1748-0221/3/08/S08004.

[2] Design, performance, and calibration of CMS hadron-barrel calorimeter wedges, Eur.Phys.J. C55 (2008) 159–171. doi:10.1140/epjc/s10052-008-0573-y.

[3] Design, performance, and calibration of the CMS Hadron-outer calorimeter, Eur.Phys.J. C57 (2008) 653–663. doi:10.1140/epjc/s10052-008-0756-6.

[4] Design, performance, and calibration of CMS forward calorimeter wedges, Eur. Phys. J. C 53 (2008) 139–166. doi:10.1140/epjc/s10052-007-0459-4.

[5] T. Zimmerman, J. R. Hoff, The Design of a charge integrating, modified floating point ADC chip, IEEE J.Solid State Circuits 39 (2004) 895–905. doi:10.1109/JSSC.2004.827808.

[6] J. Mans, J. Anderson, B. Dahmes, P. de Barbaro, J. Freeman, T. Grassi, E. Hazen, J. Mans, R. Ruchti, I. Schmidt, T. Shaw, C. Tully, J. Whitmore, T. Yetkin, CMS Technical Design Report for the Phase 1 Upgrade of the Hadron Calorimeter, Tech. Rep. CERN-LHCC-2012-015. CMS-TDR-10, CERN, Geneva, additional contact persons: Jeffrey Spalding, Fermilab, spalding@cern.ch, Didier Contardo, Universite Claude Bernard-Lyon I, contardo@cern.ch (Sep 2012).

[7] PICMG, Microtca specification, Tech. Rep. MTCA.0/R1.0 (2006).

[8] CMS HCAL Collaboration, Study of light yield and radiation hardness of scintillators for cms hcal, Tech. rep., CMS-IN-2001-022 (2001).

[9] A. Tapper, D. Acosta, CMS Technical Design Report for the Level-1 Trigger Upgrade, Tech. Rep. CERN-LHCC-2013-011. CMS-TDR-12, CERN, Geneva, additional contacts: Jeffrey Spalding, Fermilab, Jeffrey.Spalding@cern.ch Didier Contardo, Universite Claude Bernard-Lyon I, didier.claude.contardo@cern.ch (Jun 2013).